TB07

19th International Symposium of Ballistics, 7–11 May 2001, Interlaken, Switzerland

PROTECTIVE POWER OF THICK COMPOSITE LAYERS AGAINST MEDIUM-CALIBER LONG-ROD PENETRATORS

H.-J. Ernst[1], T. Wolf[1] and W. F. Unckenbold[2]

[1] *French-German Research Institute of Saint-Louis (ISL), P. O. Box 34, F-68301 Saint-Louis Cedex, France*
[2] *Invent GmbH, Abelnkarre 2a, D-38100 Braunschweig, Germany*

The ballistic protection performance of thick GFRP blocks is investigated in depth of penetration experiments with tungsten heavy alloy long rods at impact velocities of about 1800 m/s. The formerly introduced doctile limit of the equivalence factor, which sufficiently describes the protective power of brittle and ductile target materials, is successfully applied to GFRPs too. Unlike ductile or brittle materials, the ballistic resistance of a thick GFRP block grows with increasing penetration depth, and thus makes GFRP materials interesting for light-weight armor applications. The corresponding increase of the target resistance of the GFRP during the penetration process can be explained by the special anisotropic behavior of the fabric layers. The growing bulge in front of the projectile makes the tensile strength of the fibers increasingly effective in withstanding the axial load.

INTRODUCTION

Besides brittle materials, such as industrial ceramics and glass, as well as ductile metals, such as titanium, the interest of light-weight armor designers has been increasingly focused on composite materials, such as GFRP *(Glass-Fiber* Reinforced Plastic) in the last years. Therefore, a classification of the protective power of these materials will be helpful. The protective power of different inert materials against the KE threat (KE = *K*inetic *E*nergy) is generally evaluated by DOP experiments (DOP = *D*epth *O*f *P*enetration), where the penetration in the considered test target (i.e. block of GFRP material plus steel backing) is compared to the one achieved in a reference steel block of semi-infinite thickness at the same impact velocity. An appropriate analysis of these ballistic results yields equivalence factors quantifying the protective power of the material.

The constructive configuration which is often called confinement as well as the target layer thickness influence the protective power of inert materials against the given threat [1]. It is known from literature and from our own experiments that the equivalence factors of brittle materials decrease with increasing block thickness [2, 3, 4], whereas ductile materials have constant values. Furthermore, it has been shown that the protective power of

several brittle targets is all the higher as they are better confined [5, 6]. A ballistic material parameter, called ductile limit of the volume equivalence factor, has been fonnd which eliminates this configuration dependence and which allows a joint protective power ranking of brittle and ductile materials [7, 8].

This investigation has two aims: firstly, the thickness- and confinement-dependent protective power of different GFRPs is evaluated by applying the above-mentioned equivalence factor; secondly, a closer insight into the terminal ballistic behavior of thick GFRP layers under high-velocity impact loading is given.

EXPERIMENTAL DESIGN

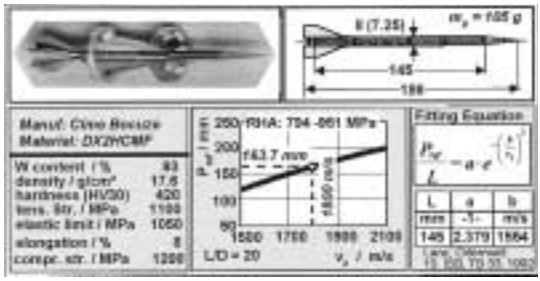

Figure 1: KE Threat BMU G 154.

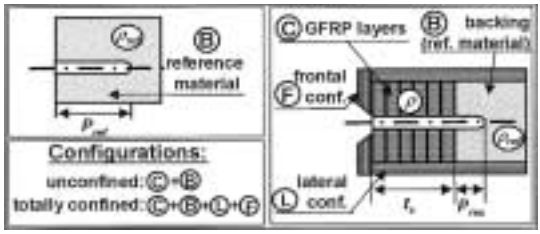

Figure 2: GFRP target for DOP experiments.

Quadraxial glass fabric	matrix material fibre material glass content / wt % density / g/cm³ tensile strength / MPa flexural strength / MPa shear modulus / GPa	VE glass 80 1.98 300 (approx.) 500 (approx.) 4
	parallel to the fibre	**orthogonal to the fibre:**
Young's modulus / GPa extensional wave velocity / m/s longitudinal wave velocity / m/s	41 4574 4965	14 2673 2901

Figure 3: GFRP material parameters.

An APDSFS projectile (APDSFS = *A*rmor *P*iercing *D*iscarding *S*abot *F*in *S*tabilized) developed at ISL is usod as KE-threat (Fig. 1). The upper pictures show a photograph of the projectile with its light metal sabots and a sectional drawing of the penetrator. The lower tables give some material parameters of the penetrator material, its reference penetration into RHA as a function of impact velocity, and the parameters of the fitting equation.

The GFRP material has been tested in two configurations, called unconfined and totally confined. Fig. 2 schematically shows the target set-up for the DOP experiments. In the unconfined configuration the GFRP block is directly placed on an RHA backing of semi-infinite thickness. In the totally confined configuration it is additionally encased in steel plates of 20 mm thickness. The hole in the front plate allows comparable impact conditions.

Layered target blocks of different thicknesses and 200-mm-thick monoblocks are investigated with lateral dimensions of 100 x 100 mm^2.

The glass fibers of the GFRP under investigation is placed into the VE matrix in the form of a quadraxial

fabric as is seen in the schematic drawing in the top left of Fig. 3. An overview of some constitutive data of the GFRP material is given in the tables to the right and below. It is important to keep in mind that the values of Young's modulus as well as the extensional and the longitudinal wave velocities have significantly different values parallel and orthogonal to the fiber directions. The anisotropic relation of both velocities is approx. 1.71. With respect to the positions of the glass fiber layers in one LOS plane of the quadraxial fabric, the axial/lateral velocity relation has an average value of 1.28.

ANALYSIS OF THE DOP EXPERIMENTS

As seen in Fig. 2, a residual penetration P_{res} is measured in the RHA backing (density ρ_{ref}) behind the investigated GFRP target (total thickness t_z, density ρ) and is compared to P_{ref}, the penetration depth of the projectile at the same velocity in the reference material of semi-infinite thickness.

After the normalization of the two parameters t_z and P_{ref} in order to eliminate the experimentally caused scattering of the impact velocity, a layer of the reference material $t_{ref,n}$ can be defined as

$$t_{z,n} = t_z / P_{ref}, \quad P_{res,n} = P_{res} / P_{ref} \quad \rightarrow \quad t_{ref,n} = 1 - P_{res,n}$$

which yields the same residual penetration P_{res}. Based on these quantities the above-mentioned ballistic space equivalence factor

$$F_S = t_{ref,n} / t_{z,n}$$

describes the volume gain of the GFRP block under consideration as compared to the reference layer. If the volume factor is multiplied by the density relation ρ_{ref}/ρ, the mass equivalence factor is obtained.

In former investigations on ceramic targets it has been found that the space equivalence factor for vanishing block thickness should have the same limit value for all configurations [7]. This hypothesis leads to an appropriate approximation algorithm based on an exponential fitting function

$$F_S = F_S(0) \cdot exp\,(\gamma \cdot t_{z,n})$$

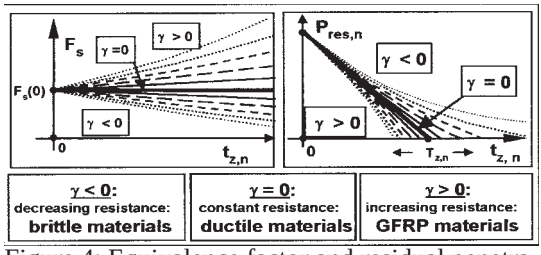

Figure 4: Equivalence factor and residual penetration for brittle, ductile and composite materials.

where $F_S(0)$ is the configuration-independent fitting parameter [8]. The approximation coefficient γ depends on both the material and the target configuration. Fig. 4 shows qualitative diagrams of the proposed approximation function F_S (left-hand side) and of the resulting $P_{res,n}$ (right-hand side) dealing with hypothetical

brittle, ductile and composite materials, in order to schematically describe different types of penetration behavior and the dependence on target configurations. The thick horizontal line in the F_S diagram marks the quasi-ductile penetration behavior which is also found in the linear relation in the $P_{res,n}$ diagram ($\gamma = 0$). The non-linear penetration curves represent brittle materials for $\gamma < 0$ (concave curves) and composite materials for $\gamma > 0$ (convex curves). High absolute values of γ indicate large differences compared to a ductile penetration behavior [5, 7].

$F_S(0)$ was found to be the highest possible value of a brittle material which equals the one occurring in an optimally confined target where the penetration behavior of a ductile material can be reached. Consequently, it was called ductile limit of the space equivalence factor for this kind of material [8].

For the GFRP material under consideration the dependence of the space equivalence factor on target thickness and confinement is analyzed with the same approximation algorithm to compare its penetration behavior to those of previously investigated ductile and brittle materials. The convex curves in Fig. 4 anticipate the results for this composite material which will be described in the following section.

RESULTS

Protective Power

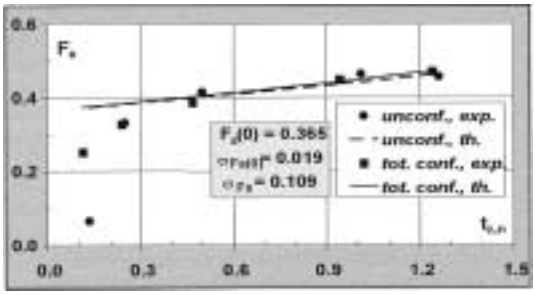

Figure 5: Volume equivalence factors as a function of material thickness.

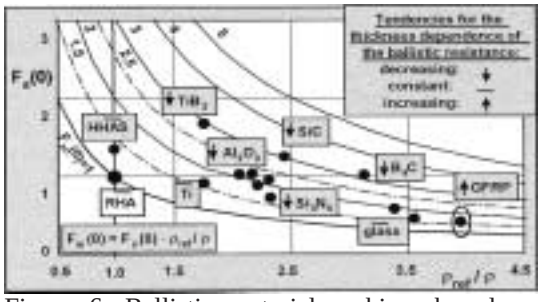

Figure 6: Ballistic material ranking, based on $F_S(0)$ valne of the space equivalence factor.

The results of the DOP experiments with the considered GFRP material are summarized in Fig. 5. The diagram shows experimentally determined ($t_{z,n}$,F_S)-data (dots) as well as fitting corves $F_S(t_{z,n})$ for the unconfined and totally confined configuration investigated.

It can be seen that the space equivalence factor increases with the target thickness in both configurations. This means that a thick composite block has a higher mean value of relative protective power than a thin one or, in another interpretation, the target resistance grows with the increasing penetration depth.

On the other hand, the $F_S(0)$ value is relatively small compared to previously investigated brittle and ductile materials which can be seen in the mterial ranking of Fig. 6. Here, the basic ballistic material parameter

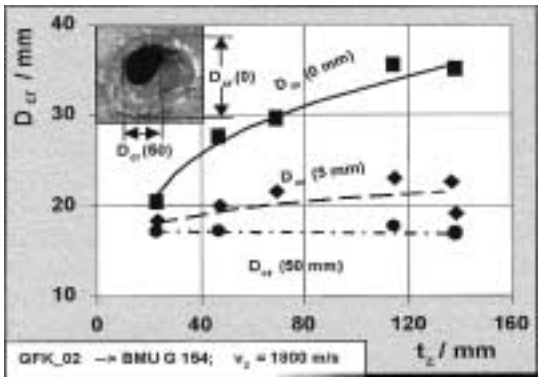

Figure 7: Crater diameters in the backing behind differently thick GFRP targets.

$F_s(0)$ is plotted versus the density relation ρ_{ref}/ρ. Both the increasing ductile limit of space equivalence and the increasing density relation indicate a growing protective power. The hyperbolic lines for $F_m(0)=const$ define different mass gain levels. It is interesting to notice hardness armor steel (HHAS), titanium the and glass have approximately the same mass-related protection level: $F_m(0) \approx 1.5$.

Therefore, GFRPs are materials which can be usefully applied to lightweight armor design.

Penetration Phenomena

It was found in the post-mortem analysis of the experiments that the entrance crater diameter in the backing behind a GFRP block is significantly larger than the crater diameter in the reference steel, as shown in the little upper photograph of Fig. 7. In the diagram of Fig. 7 the variation of the crater diameter with the increasing block thickness of the GFRP block is quantified [9, 10]. Three different diameters have been measured in the first backing plate: the surface diameter *D(0 mm),* i.e. the beginning of the crater formation in the backing, a diameter in a depth of 5 mm *D(5 mm)* (to show approximately the transition to the stationary phase of the penetration process in steel), and the exit diameter *D(50 mm)* of the first backing plate which corresponds to the generally known crater diameter in RHA. The increase of the entrance diameter *D(0 mm)* with the increasing block thickness $t_{z,n}$ may be explained by an enlarged mushrooming of the projectile during the penetration in GFRP.

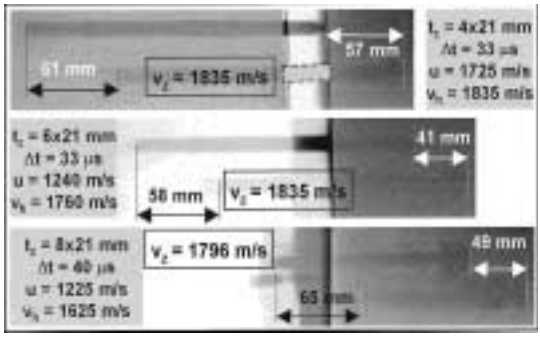

Figure 8: Double-exposed X-ray pictures of the erosion of the rod tip during the penetration into differently thick GFRP targets.

The X-ray technique offers a direct visualization of the penetration process. Fig. 8 shows double-exposed X-ray pictures of three experiments with GFRP blocks of different thickness (80 mm, 120 mm and 160 mm). The exposure times were chosen in order to observe six successive states of the ongoing mushrooming during the penetration (the second and the third exposure times as well as the fourth and the fifth ones are very close to one another). The cratering velocity *u* as well as the projectile tail velocity v_h are calculated

from the given time and space relations and assigned to each picture. The given tip displacements (57, 41 and 49 mm) correspond to the growth of the penetration depth.

The first two exposures in the upper picture show the mushroom formation after impact up to a size of approximately two projectile diameters. In the second exposure in the middle picture a clearly enlarged mushroom diameter of nearly 3D is seen. In the lower picture no significant further mushroom growth is visible. Similar mushrooming observations are reported from investigations with models of steel fragments impacting GFRP plates [9]. During the observed time intervals the average craterization velocity decreased from 1725 m/s to 1225 m/s.

The targets from which the X-ray pictures in Fig. 8 were taken consisted of stacks of GFRP plates. In the following experiments 200-mm-thick GFRP blocks have been investigated. In the left hand side of Fig. 9 photographs of the GFRP block have been taken before (upper picture) and after the experiment (lower picture). In the lower picture the state of delamination is seen. Two computer drawings reproduced from the delaminated slices represent a upper side view and a 3D view of the crater. The vertical lines in the upper side view show the post-mortem delamination gaps.

It is obvious that the crater does not follow the shot axis as can also be seen in the lower photograph, though the GFRP matenal has a relatively low may be explained by the following consideration: the X-ray pictures of Fig. 8 show an enlarged and not axially symmetric mushrooming of the projectile tip. Obviously, some parts have broken off during the tip formation. Consequently, the projectile is laterally yielding towards the direction with the smallest tip resistance thus deviating from the shot axis. The nonlinearity of the crater will also contribute to a certain extent to the thickness-dependent resistance increase of the GFRP material.

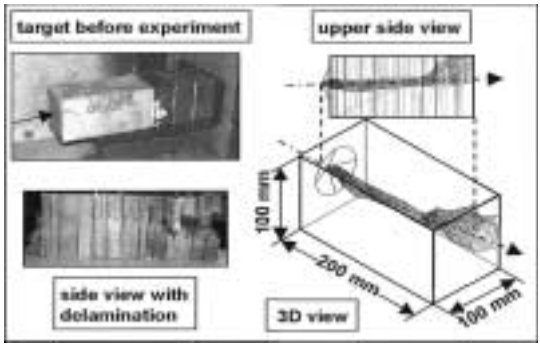

Figure 9: Postmortem views of the crater and the delamination of a 200-mm-thick GFRP target.

Penetration Mechanism

Based on these experimental results the working hypothesis of the governing mechanism of GFRP behavior under high-velocity impact loading could be confirmed. The target resistance increase during the penetration process can be explained by the special anisotropic behavior of the fabric layers. As the preferred lateral expansion of the strain wave enlarges the radial extension of the bulge, accordingly growing numbers of fiber layers of the GFRP material are incorporated into the growing bulge formation in front of the projectile which develops faster than the crater formation. Consequently, the fibers withstand the axial load by increasingly activating their tensile strength. The bulged structure stiffens and increases the penetration resistance of the incorporated material, the compliance in the axial direction being maintained. The more the projectile tip approa-

ches the backing, the more this compressibility causes an additional resistance. All these effects put together result in the growing penetration resistance which is observed in the X-ray pictures of the increased mushrooming of the projectile tip.

CONCLUSIONS

The considered GFRP has shown growing equivalence factors with increasing target thickness in contrast to brittle and ductile materials.

The increasing mushrooming of the projectile tip within thick GFRP blocks has been verified. The corresponding increase of the target resistance of the GFRP during the penetration process can be explained by the special anisotropic behavior of the fabric layers. The growing bulge in front of the projectile makes the tensile strength of the fibers more effective in withstanding the axial load.

The curved penetration channel may be caused by the fact that some parts of the projectile tip have broken off during the tip formation. Consequently, the projectile is laterally yielding towards the direction with the smallest tip resistance. This nonlinearity of the crater will additionally contribute to the thickness-dependent resistance increase.

Thick GFRP blocks reach the protective potential of titanium. Therefore, and taking into account all the ballistic results available today, it is obvious that thick layers of GFRP are useful for lightweight armor design.

REFERENCES

1. Westerling L., Lundberg T., "The Influence of Confinement on the Protective Capability of Ceramic Armour at Two Different Velocities", *15th Int. Symp. on Ballistics*, Jerusalem, Israel, Vol. 1, 283–290, 1995
2. Andersen Jr. C.E., Walker J.D., Lankford J., "Investigations of the Ballistic Response of Brittle Materials", *SWRI-Technical Report*, 1995
3. Yaziv D., Partom Y., "The Ballistic Efficiency of Thick Alumina Targets against Long Rod Penetrators", *14th Int. Symp. on Ballistics*, Quebec, Canada, Vol. 2, 331–340,1993
4. Hauver G.E., Netherwood P.H., Benck A.F., Gooch W.A., Perciballi W.J., Burkins M.S., "Variation of Target Resistance During Long-Rod Penetration into Ceramics", *13th Int. Symp. on Ballistics*, Stockholm, Sweden, Vol. 3, 257–264, 1992
5. Ernst H.-J., Hoog K., Wiesner V., "Ballistic Impact Behaviour of Some Ceramics in Different Environments", EURODYMAT 94, Oxford, UK, *J. Phys. IV, Coll. C8, Suppl. J. Phys III*, Vol. 4, 677–682, 1994
6. Rupert N.L., Grace F.E., "Penetration of Long Rods into Semi-infinite, Bi-element Targets", *14th Int. Symp. on Ballistics*, Quebec, Canada, Vol. 2, 469–478, 1993
7. Hoog K., Ernst H.-J., Wolf T., "A New Parameter Characterising the Ballistic Performance of Ceramics", EURODYMAT 97, Toledo, Spain, *J. Phys. IV France 7, Coll. C3, Suppl. J. Phys. III*, 241–2461, 1997
8. Hoog K., Ernst H.-J., "Ductile Limit of the Ballistic Response of Steel Backed Ceramics", *17th Int. Symp. on Ballistics*, Midrand, South-Africa, Vol. 3, 57–64, 1998
9. Ernst H.-J., Hoog K., Wolf T., "Penetration Performance of Composite Materials and Composite Structures", *ISL PU 349/99*, 1999
10. Ernst H.-J., Wolf T., Hoog K., Unckenbold W.F, "GFRP Materials under High-Velocity Impact Loading", EURODYMAT 2000, Cracow, Poland, *J. Phys. IV,* Vol. 10, Pr9 577–582, 2000